*Journal of The Electrochemical Society*, **149** (12) A1610-A1615 (2002)
0013-4651/2002/149(12)/A1610/6/$7.00 © The Electrochemical Society, Inc.

# Block Copolymer-Templated Nanocomposite Electrodes for Rechargeable Lithium Batteries

**S. C. Mui,[a,*] P. E. Trapa,[a,*] B. Huang,[a] P. P. Soo,[a] M. I. Lozow,[a] T. C. Wang,[b] R. E. Cohen,[b] A. N. Mansour,[c,**] S. Mukerjee,[d,**] A. M. Mayes,[a,**] and D. R. Sadoway[a,**,z]**

[a]*Department of Materials Science and Engineering,* [b]*Department of Chemical Engineering, Massachusetts Institute of Technology, Cambridge, Massachusetts 02139-4307, USA*
[c]*Naval Surface Warfare Center, Carderock Division, West Bethesda, Maryland 20817-5700, USA*
[d]*Department of Chemistry, Northeastern University, Boston, Massachusetts 02115-5000, USA*

A self-organizing, nanocomposite electrode (SONE) system was developed as a model lithium alloy-based anode for rechargeable lithium batteries. *In situ* X-ray adsorption spectroscopy, galvanostatic testing, cyclic voltammetry, X-ray diffraction, and transmission electron microscopy were used to analyze the electrode, which was fabricated from a polyethylene oxide-based block copolymer, single-walled carbon nanotubes, and gold salt. Processing involved a single mixing step without need of a reducing agent. It was found that thermodynamic self-assembly of the block copolymer could provide a template for incorporation of both the gold salt and nanotubes. Electrochemical testing and subsequent analysis showed that owing to the small particle size and the surrounding block copolymer matrix, the SONE system could cycle over 600 cycles with rates varying between C/1.8 and 8.8C with little evidence of decrepitation or coarsening.
 [DOI: 10.1149/1.1518482] 

Manuscript submitted February 6, 2002; revised manuscript received June 13, 2002. Available electronically October 31, 2002.

## Background

In the context of rechargeable lithium batteries, the search for high capacity anodes that avoid the safety concerns associated with pure Li metal while offering higher specific capacities than graphite has led to intense interest in lithium-alloying metals.[1-4] While some lithium alloys such as Li-Sn have high theoretical capacities (>990 mAh/g), general problems remain, including decrepitation (or crumbling) due to volume excursions, subsequent capacity fade with deep cycling,[5] kinetic limitations with lithium diffusion in alloys,[6] the need for elevated temperatures in alloying bulk samples,[7] and irreversible capacity loss.[8] Strategies to counter these problems have included reducing diffusion distances via use of nanoscale particles,[9] adding dispersive media (*e.g.*, composite oxides),[10] partial reduction,[11] employing ternary intermetallic compounds ($Li_xMM'$),[12] and using conversion reactions.[6] High surface area, nanoscalar materials have received considerable attention as lithium alloy electrodes, partly due to their ability to enhance capacity, delay cycling failure, and increase the chemical reactivity for alloying.[7,13-17]

Exploiting organic materials for directing the assembly of nanostructured, inorganic phases, offers a novel strategy for designing lithium alloy-based anodes. In some cases, polymers can provide a useful template from which to access chemical or physical properties that are scale dependent or morphologically influenced. Nanoscale templating of inorganic phases using block copolymers has previously been employed in fabricating novel magnetic, electronic, and optical materials.[18-25] Cohen and co-workers first synthesized metal nanoclusters in microphase-separated diblock copolymers by using organometallic complexes covalently incorporated into one block component.[19,20] Later, this group extended their work to develop more universal reactor schemes for synthesizing metal nanophases in preferred block copolymer domains.[21,22] Spatz *et al.* exploited the self-assembly of polystyrene-*b*-poly(ethylene oxide) micelles to form ordered arrays of gold nanoclusters that were reduced from $LiAuCl_4$.[23] The Au cluster size was found to be controllable by varying the ratio of gold salt to ethylene oxide units. More recently, Brown and Watkins demonstrated selective metallization of diblock copolymers via the reduction of organometallic precursors in supercritical $CO_2$ fluid, which preferentially swelled one of the block components.[26]

Others have created arrays of inorganic nanostructures using either ''track-etch'' polymeric membranes or porous alumina membranes as templates, rather than block copolymers.[27,28] Martin and co-workers showed that the membrane-based approach could be used to form micro- and nanoscale ''brush'' electrodes for lithium batteries. Their work demonstrated the ability to fill such templates with metals, carbon, or oxides through a variety of approaches, including sol-gel processing, electrodeposition, electroless plating, and chemical vapor deposition.[29-34]

Attention to nanoscalar approaches for electrodes has also been extended to carbon-based anodes, including recent work using carbon nanotubes as energy storage materials.[35-42] Smalley *et al.* reported single-walled carbon nanotubes (SWNTs) with reversible Li capacities of roughly 460 mAh/g ($Li_{1.23}C_6$), while Zhou *et al.* demonstrated Li capacities of 1000 mAh/g ($Li_{2.7}C_6$) following postsynthesis treatment.[36,41,42] These large capacities are offset somewhat, however, by the high processing cost of SWNTs compared to that of graphite, as well as significant initial, irreversible capacity loss. Coupling the templating capabilities of block copolymers with metal salts and nanotubes to form hybrid systems could help reduce the cost burden of nanotubes while endowing the anode with favorable electrochemical and processing features.

In this work, we investigate an anode comprising nanoscale, lithium-alloying metal particles, SWNTs and a Li-ion conducting block copolymer (BC) as an example of a self-organizing nanocomposite electrode (SONE). We demonstrate the utility of BCs as templates for forming nanostructured materials with electrochemical functionality. Used as structure-directing agents, BCs can be designed to disperse and localize the electrode components within specific domains. The templating ability of BCs obviates the need for preliminary nanoparticle synthesis, subsequent reduction agents, or multiple mixing steps in fabricating nanoscale composite electrodes for rechargeable lithium batteries.

The use of a block copolymer matrix to obtain improved electrochemical performance is also evaluated. Thomas and Newman suggest that to mitigate capacity fade in alloy electrodes, the design must involve little volume change or provide a driving force to keep particles together during contraction, must prevent resistive layers from forming during alloy expansion and contraction, and must inhibit agglomeration of particles.[43,44] Electrochemically, BCs may help render the electrode less susceptible to solid electrolyte interphase (SEI) formation at low potentials while inhibiting agglomera-

* Electrochemical Society Student Member.
** Electrochemical Society Active Member.
z E-mail: dsadoway@mit.edu

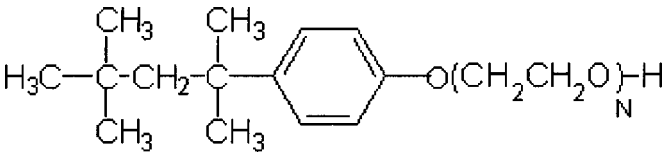

**Figure 1.** Structure of Triton X-100 surfactant used to disperse the SWNTs in water. $N \approx 9.5$.

tion of metal particles, thereby averting large volume excursions. The BC matrix was also envisioned as an elastic binder, sequestering Au particles with the SWNTs, and absorbing their expansion and contraction without matrix fracture.

The block copolymer poly(methyl)methacrylate-*b*-poly(oxyethylene)$_9$ methacrylate, PMMA-*b*-POEM, was used to provide dimensional stability to the composite anode and establish ionic and electronic contact between a metal dispersion of Au nanoparticles generated *in situ*, carbon nanotubes, and a liquid electrolyte. While the BC used here played multiple roles as a template, binder, and ionic conductor, lithium-salt-doped BCs have also been applied for use as solid polymer electrolytes in rechargeable lithium batteries.[45-50] Ultimately, such electrolytes could be employed with SONEs of the type studied here, providing a seamless interface between battery components.

Gold was selected as the alloying component for this model system owing to its nobility (inability to form an oxide surface film) and its ability to alloy with lithium ($Li_{3.75}Au$).[51] Incorporation of gold particles into the ionically conducting block copolymer domains occurs during *in situ* metallothermic reduction of a gold-bearing salt. SWNTs were utilized to electronically connect or ''wire'' the gold dispersion to the external circuit. The resulting anodes exhibited no evidence of decrepitation or coarsening and demonstrated excellent resistance to capacity fade when cycled at high current densities.

## Experimental

The SONE was prepared by solvent casting a suspension of PMMA-*b*-POEM (58.1 wt %), polyethylene glycol dimethyl ether (PEGDME, 17.4 wt %, $M_n$ = 430 g/mol, Polysciences), SWNTs (10 wt %, obtained courtesy of Rice University), and $LiAuCl_4 \cdot xH_2O$ (14.5 wt %, 99.99% purity on a metals basis, Alfa Aesar), using tetrahydrofuran (THF) as the solvent. Synthesis of the BC used in this study has previously been described.[47] The PMMA-*b*-POEM copolymer was 49:51 (v/v) in composition and had a number average molecular weight, $M_n$, of 77,200 g/mol. The BC and PEGDME were dissolved in THF followed by the introduction of the Au salt. To this mixture, SWNTs in the form of a water suspension were added and stirred for approximately 2 h. Part of the mixture was cast onto a glass plate and allowed to air dry, followed by further drying in a vacuum oven at 80°C for 48 h. The dried film was transferred to an argon-filled glove box and peeled off its substrate. The film was sectioned into electrodes, approximately 1 mg in weight and 0.2 cm$^2$ in area.

SWNTs self-assemble into bundles of approximately 10-50 nm in diam, which consist of approximately 30-600 individual tubes, each 1.4 nm in diam. Prior to their receipt, processing of the nanotubes involved coating post acid-treated bundles with the surfactant Triton X-100 (Fig. 1), an octylphenol ethylene oxide condensate with a hydrophobic head that adsorbs on the nanotube surface and a hydrophilic (EO)$_9$ tail that facilitates their dispersion in water.[42] In the fabrication of the nanocomposite electrode, the presence of this surfactant coating provides a mechanism to corral the nanotubes into the POEM block domains in contact with the gold salt.[52,53] This preferential localization is expected since the SWNT surfactant chemistry is close to that of the polar POEM component. Indirect evidence for such localization is also given by the electrochemical activity of the SWNTs and Au, implying that (*i*) the gold resides in the $Li^+$ conducting POEM block, (*ii*) the SWNTs also contact POEM, and (*iii*) the SWNTs supply electrons to the gold. Elemental analysis (Quantitative Technologies, Inc.) of the nanotubes revealed the presence of residual catalytic impurities of Co (0.26 wt %) and Ni (0.25 wt %) used in the SWNT synthesis.[42] Subsequent mass balance calculations and cyclic voltammetry (CV) measurements confirmed that the electrochemical contributions from these impurities were negligible.

Cells were fabricated in an argon-filled glove box with the SONE serving effectively as the cathode against an excess of Li metal (Alfa-Aesar, 30 mil thickness). Liquid electrolyte (1 M $LiPF_6$ in ethylene carbonate: dimethyl carbonate, 1:1; EM Science) was used with a separator (Celgard 2300, Celgard, Inc., Charlotte, NC). Cells were subjected to galvanostatic testing using a Maccor Series 4000 automated test system, with voltage limits of 0 and 2.5 V and currents of 50-800 μA, always at identical instant rates of charge and discharge ($i_c = i_d$).

To confirm the reduction and alloying processes involved, CV was performed on working electrodes of pure metallic Au and of SWNTs with lithium metal serving as counter and reference electrodes. All CV test cells were constructed in an argon-filled glove box, sealed, and tested outside at ambient temperature using a Solartron 1286 electrochemical interface (Solartron Analytical, Houston, TX) controlled by Corrware/Corrview (Scribner Associates, Inc., Southern Pines, NC). The SWNTs were scanned in a potential window of 0.0 to 3.0 V at scan rates from 0.5 to 10 mV s$^{-1}$. For the Au working electrode, several potential windows between 0.0 and 7.0 V were analyzed at 200 mV s$^{-1}$ to verify the alloying process.

Wide-angle X-ray scattering (WAXS) and peak-breadth determination were performed on early-cycled and postcycled samples to evaluate Au crystallite sizes, using a rotating anode X-ray powder diffractometer (Rigaku Corp., Tokyo, Japan) and JADE 6$^+$ analysis software (Materials Data, Inc., Livermore, CA). Diffraction patterns were obtained using Cu Kα radiation and rotating the SONE samples by an angle θ and the detector by 2θ (Bragg-Bretano diffraction). Transmission electron microscopy (TEM) was performed on solvent cast films of PMMA-*b*-POEM doped with Au salt using a JEOL 200CX in bright-field mode operating at 200 keV.

*In situ* X-ray absorption spectroscopy (XAS) was used to investigate the reduction and alloying process over the first discharge of the cell. The XAS experiments were conducted on beamline X-11A of the National Synchrotron Light Source (NSLS) at Brookhaven National Laboratory with the electron storage ring operating at an energy of 2.8 GeV and a current in the range 110-250 mA.[54] Spectra of the Au $L_3$-edge (11919 eV) were collected in transmission mode at room temperature using a Si(111) double-crystal monochromator (detuned by 15%). The X-ray intensities were monitored using ionization chambers filled with a flowing mixture of nitrogen ($N_2$) and argon (Ar) gases. The mixing ratio for the two gases was adjusted to yield 20% absorption for the incident beam and 60% absorption for the transmitted beam. Data were collected with energy intervals per step of 5 eV for the pre-edge region (11618-11888 eV), 0.5 eV for the edge region (11888-11968 eV), and a *k*-space interval of 0.05 Å$^{-1}$ for the remainder of the spectrum. Each spectrum extended to 13021 eV for the *in situ* electrode data and 13448 eV for the Au foil data. Integration intervals per point were set to 1 second for the pre-edge and edge regions and 2 s for the postedge region. A delay time of 0.3 s was used between successive data points in order for the monochromator to equilibrate at each point. The energy of the monochromator was calibrated using a 5 μm thick Au foil with the edge energy of 11918 eV assigned to the inflection point of the main edge. The *in situ* spectra for the electrode were collected simultaneously with the spectrum for the Au foil to continuously monitor the energy calibration of the monochromator. In this case, the intensity of the transmitted beam through the reference Au foil was measured using a third ion chamber containing the same mixture as that used for monitoring the transmitted beam through the electrochemical cell. Each spectrum required an acquisition time of 21 (for the

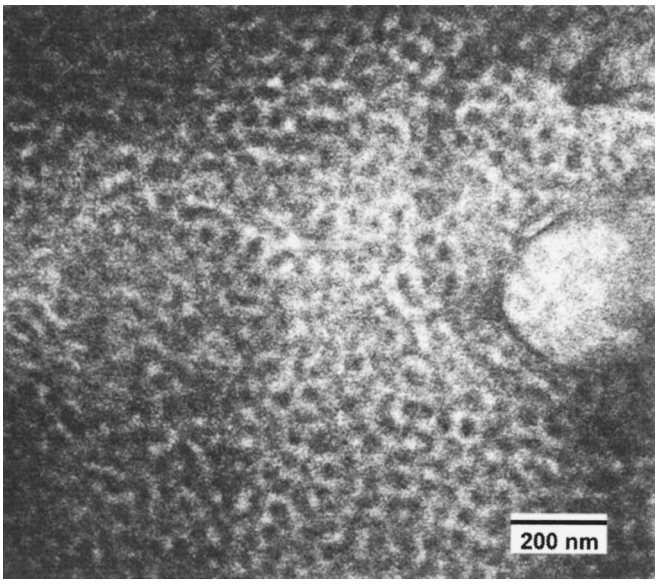


**Figure 2.** TEM image of microphase-separated PMMA-*b*-POEM after addition of 20 wt % $LiAuCl_4$. Localization of this Au salt to the POEM component (dark regions) provides contrast between the block domains.

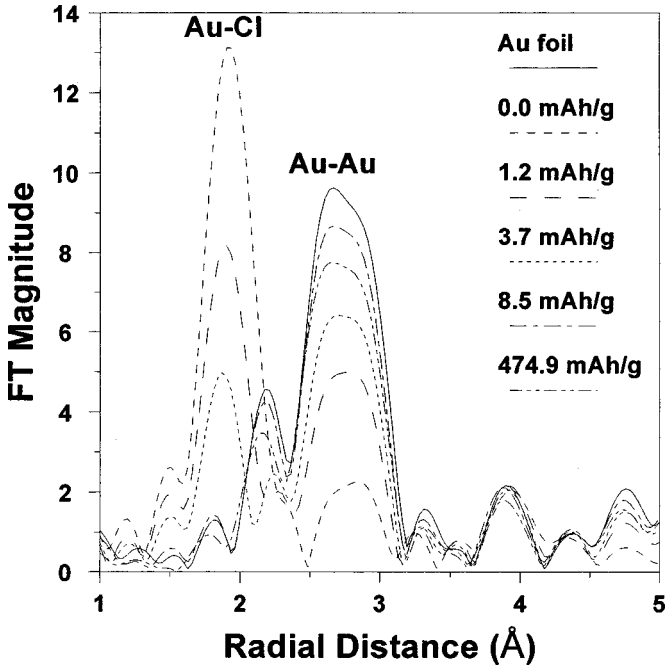


**Figure 3.** Phase uncorrected Fourier transforms of $k^3$-weighted *in situ* EXAFS data of $LiAuCl_4$ reduction and subsequent alloying with increasing discharge time along with that for metallic Au over the *k*-space range 3.0-14.0 $Å^{-1}$ and a Hanning window of 0.5 $Å^{-1}$. Note that distances in these Fourier transforms are shifted by roughly −0.2 Å from the actual distances.

electrode) and 24 (for the Au foil) minutes. The Au $L_3$-edge jumps are 0.81 (for the electrode) and 1.08 (for the Au foil). The EXAFS (extended X-ray absorption fine structure) spectrum, $\chi(k)$, was extracted using a cubic spline procedure, which minimized the amplitude of nonphysical peaks in the 0-1 Å region of the Fourier transform.[55,56] The photoelectron wavenumber, *k*, was defined by assigning the inflection point as the zero of the photoelectron energy. The spectra were normalized to a per atom basis using the absorption edge jump at 100 eV above the edge energy. Energy dependent normalization was also applied to the $\chi(k)$ data using the atomic absorption calculated with McMaster coefficients.[57]

## Results and Discussion

The ability of the block copolymer to template the alloying metal component of the nanocomposite electrode is demonstrated in Fig. 2, which shows a bright field TEM image of PMMA-*b*-POEM doped with $LiAuCl_4$ (~20 wt %). As shown in a previous investigation, incorporation of a lithium salt induces microphase separation of the otherwise miscible PMMA and POEM block components.[48] In Fig. 2, contrast between the microphase-separated block domains arises from localization of the electron-dense Au salt to the POEM domains (darker regions). Extended exposure to high energy electrons in the TEM causes the $LiAuCl_4$ to be reduced *in situ*, leaving discrete nanometer-scale particles dispersed through the POEM domains of the block copolymer.[58] The morphology of the salt-containing block copolymer in Fig. 2 appears to be a bicontinuous gyroid structure.[59] Addition of other components to the block copolymer, including SWNTs, PEGDME, and liquid electrolyte might be expected to shift the equilibrium morphology to one of higher effective POEM content, preserving the continuity of the POEM domains.[59,60] While the *in situ* morphology was not ascertained in this investigation, the electrochemical data provides indirect evidence that a continuous structure is indeed present, with the POEM block domains serving as pathways for ionic conduction through the electrode. Addition of the surfactant-coated carbon nanotubes to the BC/salt provides a mechanism for the *in situ* reduction of the $LiAuCl_4$ salt upon electrochemical cycling.

Confirmation of Au salt reduction on cycling was obtained via XAS performed *in situ* during the initial discharge of the cell. Figure 3 shows that, upon initial discharge, the amplitude of the Au-Cl peak at ~1.9 Å rapidly diminishes while the Au-Au peak at ~2.75 Å increases, signaling the formation of metallic gold. This latter peak reaches a maximum and then decreases with further discharge, apparently due to the onset of Au-Li alloying. We conclude that metallic gold is being produced by reaction between the $LiAuCl_4$ and lithium metal generated by faradaic reduction of $Li^+$. The reduction of the gold salt shown by the EXAFS data also suggests that the SWNTs are in intimate electronic contact with the salt-doped POEM domains and thus serve as electron carriers. The localization of the Au within the POEM domains (Fig. 2), in conjunction with the preference of the Triton-coated SWNTs for the hydrophilic POEM block, support the conclusion that the active electrode components self-assemble in the ion-conducting domains of the block copolymer.[52,53]

The galvanostatic testing and resulting voltage profiles are consistent with the EXAFS results above, which suggest Li-Au alloying. Long-term cycling of the SONE system between 0.0 and 2.5 V at several current rates illustrates the reversibility of the alloying reaction (Fig. 4). An initial large drop in capacity was attributed to the reduction of the Au salt and the irreversible capacity loss associated with the high surface area SWNTs.[42] Initial cycling was performed at 50 μA (43.5 mA/g electrode) and increased stepwise to 800 μA (696 mA/g electrode) by the 210th cycle. The discharge and charge rates were subsequently lowered to the original values and finally to 25 μA after 520 cycles. The cell shows good cyclability and high rate capability up to 700 cycles, with the onset of significant capacity fade after ~600 cycles. After 720 cycles, cycling was stopped and the cell disassembled in an argon-filled glove box for post mortem analysis.

Wide-angle X-ray scattering was performed to assess Au crystallite size in the SONE sample that had been cycled 720 times and another cycled only four times. Both samples were stopped in the fully charged state, in which the samples are completely dealloyed, in order to access evidence of coarsening or deterioration of the Au crystal structure under the deep cycling conditions. X-ray diffraction (XRD) patterns for both samples, shown in Fig. 5, reveal seven peaks attributed to Au. Rietveld refinements and subsequent crystal-

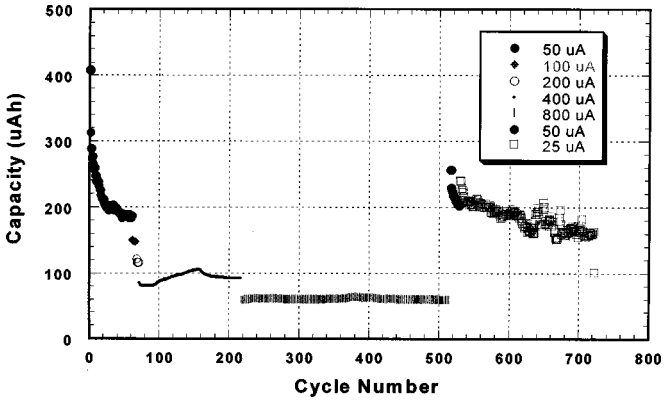


**Figure 4.** Cycling of SONE electrode *vs.* lithium metal at various discharge rates. Key shows sequence of current rates applied.

lite size determination using peak-breadth measurements revealed average crystallite sizes of 30-35 nm for both samples (limited and fully cycled), suggesting that the Au particles remain confined to the nanoscale POEM domains of the block copolymer, and that coarsening of the Au particles upon cycling was minimal. WAXS analysis reveals somewhat different peak intensity ratios for SONE samples cycled 4 and 720 times, with $I_{111}/I_{200} \simeq 3.05$ and 2.25, respectively. For both samples, $I_{111}/I_{200}$ is higher than the referenced value of 1.92, suggesting that the nanoparticles grow in a preferred orientation. The mechanism responsible for this orientation can only be speculated at this point.

Differential capacity plots were used to analyze the cycling characteristics of the electrode. Figure 6 reveals the presence of several discharge and charge plateaus (observed as peaks) representing two-phase regions during lithium alloying. The charging peaks located at approximately 0.18, 0.48, 0.74, and 1.15 V are believed to be associated with dealloying of the $Au_4Li_{15}$, $AuLi_3$, $\delta_1$ ($\sim AuLi_2$), and $\beta$ ($\sim$AuLi) phases, respectively.[51] The scale has been resized to emphasize the lithium alloying peaks relative to the SWNT background. The large electrochemical background contributed from the SWNTs was also studied (discussed below) and is not correlated with the observed peaks, which were attributed to reversible Au-Li alloying. Upon discharge, only the corresponding peaks associated with the onset of the $\beta$, $\delta_1$, and $Au_4Li_{15}$ phases are initially observed. By the 50th discharge cycle, only the first two discharge peaks are observed ($\beta$ and $\delta_1$) while all four peaks remain evident in the corresponding charge cycle, albeit depressed (Fig. 8). This suggests that traversing the phase diagram in the charge direction (*i.e.*, the removal of lithium) may be more kinetically facile than the discharge process (alloying) upon reaching the latter two phases ($AuLi_3$ and $Au_4Li_{15}$).

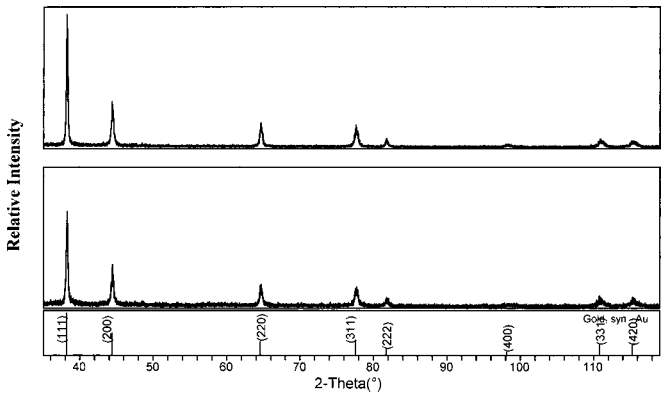


**Figure 5.** Wide-angle X-ray diffraction patterns of SONE samples cycled 4 times (top) and 720 times (bottom). Peak fits reveal an average crystallite size of 30-35 nm in each case.

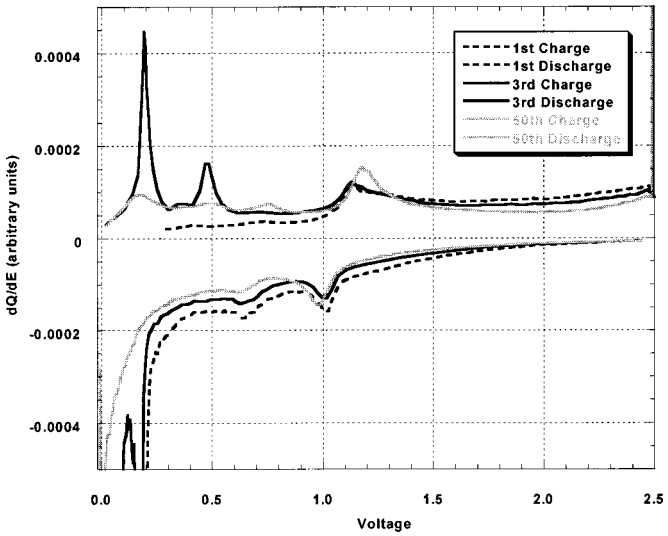


**Figure 6.** Differential capacity plots of the first, third, and 50th cycles ($I_c = I_d = 50\ \mu A$). The discharge sweep (bottom) represents alloying while the charge sweep (top) represents dealloying. The four peaks in the charge sweep are associated (from left to right) with the phase transformations from $Au_4Li_{15}$, $AuLi_3$, $\delta_1$($\sim AuLi_2$), and $\beta$ ($\sim$AuLi), respectively. Peaks below 0.5 V on discharge are partially cropped because of scaling and large hysteresis from SWNTs.

Calculation of the volume expansion of the Au upon Li alloying requires estimation using the Au-Li phase diagram, accounting for the structure, lattice parameters, and atomic arrangement of Au and Li atoms.[61-64] At high temperatures in the $\alpha$ phase (a distorted face-centered cubic structure), the lattice parameter changes from 4.079 (Au) to 3.968 (39.2 atom % Li), representing an overall 22% volume expansion upon traversing the entire phase. One might expect a comparable volume change at room temperature across this range of composition, although the precise value will depend on the adopted structure. For the $\beta'$ phase ($\sim$55 atom % Li) exhibiting a CsCl structure, Kienast and Verma reported a density of 10.10 g/cm$^3$.[65] This translates to a doubling of the initial nanoparticle volume in the nanocomposite anode.[65] Small particle sizes, together with a matrix that prevents agglomeration, appear instrumental in allowing such large volume excursions to occur without immediate capacity fade.

For comparison, an electrode incorporating bulk Au powder, carbon black, and poly(vinylidene fluoride) as binder was prepared and run under similar galvanostatic conditions. Cells were cycled approximately 100 times before significant capacity fade was observed. Differential plots of these cells (not shown) also revealed voltage plateaus corresponding with the onset of the $\beta$($\sim$ AuLi) and $\delta_1$ phases. The peaks associated with onset of the $AuLi_3$ and $Au_4Li_{15}$ phases were not observed, presumably due to transport limitations in these bulk powders under the chosen test conditions. Independent cyclic voltammetry performed on a gold working electrode of 2.3 mm$^2$ against lithium counter and reference electrodes revealed a single peak in the anodic sweep close to the 1.1 V peak observed for the SONE system. Obtaining the additional alloying peaks in the Au working electrode, however, required initially refreshing the surface of Au via electrochemical deplating at high potentials (greater than +4.0 V). Considering the practical voltage limits used for galvanostatic testing of the SONE system (0 to 2.5 V), the Au particle surface in the system could be assumed to consist of a SEI layer which develops with alloying.[66] The decrease in the peaks attributed to the $\delta_1$, $AuLi_3$, and $Au_4Li_{15}$ phases with cycling in the SONE system might also be explained by a similar passivat-

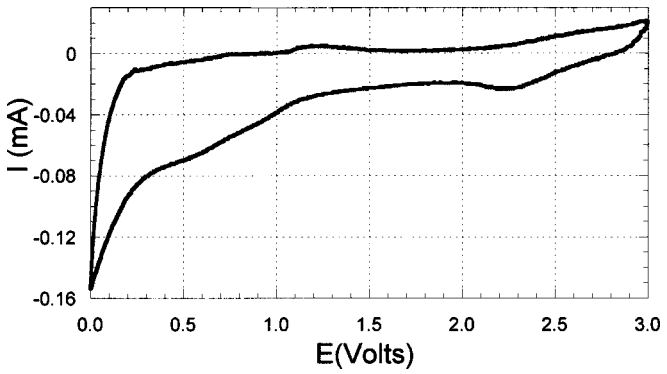


**Figure 7.** CV plot of SWNTs, eighth cycle, 0.5 mV/s.

ing layer that restricts further lithiation and phase transformation.

The large background hysteresis observed in the differential plot of the SONE system was resolved by CV on the SWNTs. A free-standing film of SWNTs was prepared by solvent casting and oven and vacuum drying nanotubes dispersed in water. Tests were performed by immersing part of the SWNT film in the same liquid electrolyte as that used for the SONE system. The eighth scan is displayed in Fig. 7, showing the absence of current peaks associated with voltage plateaus. The lack of well-defined interstitial sites has been used to explain this wide potential range for intercalation and deintercalation.[36] Previous literature has also confirmed large irreversible losses for SWNTs, ranging from 660 to 1200 mAh/g, depending on their prior treatment.[41] The CV curve in Fig. 7 overlays well with the differential capacity plot in Fig. 6 and explains the hysteresis observed in the capacity. Contributions from the residual traces of Ni/Co catalysts (~0.5 wt % of the SWNTs) used to synthesize the SWNTs were undetectable in the voltammetric traces. CV was also performed on the BC and showed no electrochemical capacity for the voltage limits used herein.[47]

Figure 8 overlays the 50th and 520th cycles of the SONE, demonstrating the reversible nature of the system after extended cycling at high current rates. The β charge and discharge peaks remain largely unchanged, showing that the lithiation process is highly reversible for $Li_xAu$ ($x = 0$ to 1). At currents above 50 μA, this peak diminishes until it completely disappears at $I_c = I_d = 800$ μA, showing that the alloying process is kinetically limited at high rates (~8.8C) even for nanocrystallites. A conservative estimate of the C rates can be obtained by assuming a weighted, theoretical capacity of ~434 mAh/g (active mass), based on $Li_xAu$ ($x = 3.75$) and $Li_yC_6$ ($y = 1$). A 50 μA current rate would then correspond to a ~C/1.8 rate and a 800 μA current rate to a ~8.8 C rate. The capacity at this high C rate can be attributed primarily to the SWNTs.

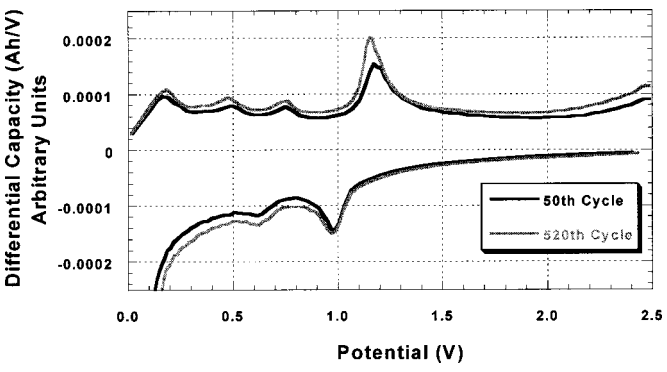


**Figure 8.** A differential capacity plot comparing the SONE Li-Au alloying peaks after extended cycling.

Calculating the peak areas at the lower C/1.8 current rate attributable to gold-lithium alloying for the 50th cycle and comparing this to the total capacity shows that the gold contributes roughly 15% of the total capacity in the electrode, mainly due to the low metal loading. Based on the weight and capacity of the microelectrode, this corresponds to roughly 314 mAh/g Au contribution, or on average ~2.3 Li per Au atom. This value correlates well with data showing one full β peak after several hundred cycles and three additional but depressed peaks ($\delta_1$, $AuLi_3$, $Au_4Li_{15}$). The presence of the alloying process after several hundred cycles without loss of capacity suggests that the gold particles are not suffering from decrepitation problems and that the SWNTs serve to electronically wire the particles.

## Conclusion

In this study, a self-organizing nanocomposite electrode was prepared as a model anode for rechargeable lithium batteries that incorporated SWNTs and Au particles as active electrode materials in an ion-conducting block copolymer binder. The choice of a block copolymer electrolyte as a matrix and template was rationalized as an approach to increase the cell's longevity by decreasing coarsening problems associated with traditional bulk composite electrodes through the confinement of metal particles and nanotubes to the ion-conducting block domains. This control over morphology on the nanometer scale allows tailoring of the macroscopic mechanical and electrical properties, providing sufficient electronic and ionic conductivity while maintaining intimate contact between the SWNTs and Au.[52,53]

Future designs of electrode systems exploiting the concept of self-organization will require increased metal loading while maintaining processing ease. Given sufficient percolation of metallic nanoparticles, adequate electronic conductivity could be obtained through direct contact or tunneling, eliminating the need for carbon. Alternately, strategies that form continuous inorganic nanophases through use of BC templates might simultaneously address this dual challenge,[22,24-26] yielding high capacity electrodes able to withstand high rates while retaining the cyclability observed herein.

## Acknowledgments

This work was sponsored by the Office of Naval Research under contracts N00014-99-1-0561, N00014-99-1-0565, and N00014-00-WX-2-0198, the Naval Surface Warfare Center Carderock Division ILIR Program, the MRSEC Program of the National Science Foundation under award DMR 98-089431, and Intronics Corp. The authors acknowledge R. E. Smalley's lab at Rice University for supplying SWNT samples under ONR contract N00014-98-1-0893.

*Massachusetts Institute of Technology assisted in meeting the publication costs of this article.*

## References

1. N. P. Yao, L. A. Heredy, and R. C. Saunders, *J. Electrochem. Soc.*, **118**, 1039 (1971).
2. R. A. Sharma and R. N. Seefurth, *J. Electrochem. Soc.*, **123**, 1763 (1976).
3. N. C. Li, C. R. Martin, and B. Scrosati, *Electrochem. Solid-State Lett.*, **3**, 316 (2000).
4. J. Wang, P. King, and R. A. Huggins, *Solid State Ionics*, **29**, 185 (1986).
5. J. Yang, Y. Takeda, N. Imanishi, and O. Yamamoto, *J. Electrochem. Soc.*, **146**, 4009 (1999).
6. R. Huggins, in *Handbook of Battery Materials*, J. O. Bessenhard, Chap 4, Wiley-VCH, Cambridge, U.K. (1999).
7. B. Gao, S. Sinha, L. Fleming, and O. Zhou, *Adv. Mater.*, **13**, 816 (2001).
8. I. A. Courtney and J. R. Dahn, *J. Electrochem. Soc.*, **144**, 2045 (1997).
9. L. F. Nazar, G. Goward, F. Leroux, M. Duncan, H. Huang, T. Kerr, and J. Gaubicher, *Int. J. Inorg. Mater.*, **3**, 191 (2001).
10. Y. Idota, T. Kubota, A. Matsufuji, Y. Maekawa, and T. Miyasaka, *Science*, **276**, 1395 (1997).
11. P. Limthongkul, H. Wang, and Y. M. Chiang, *Chem. Mater.*, **13**, 2397 (2001).
12. J. T. Vaughney, K. Kepler, C. S. Johnson, T. Sarakonsri, R. Benedek, J. O'Hara, S. Hackney, and M. M. Thackeray, in *Intercalation Compounds for Battery Materials*, G. A. Nazri, T. Ohzuku, and M. Thackeray, Editors, PV 99-24, p. 280, The Electrochemical Society Proceedings Series, Pennington, NJ (1999).
13. M. Doyle, T. E. Fuller, and J. Newman, *J. Electrochem. Soc.*, **141**, 1 (1994).
14. J. Yang, M. Winter, and J. O. Besenhard, *Solid State Ionics*, **90**, 281 (1996).

15. H. Li, X. J. Huang, L. Q. Chen, Z. G. Wu, and Y. Liang, *Electrochem. Solid-State Lett.*, **2**, 547 (1999).
16. C. S. Wang, A. J. Appleby, and F. E. Little, *J. Power Sources*, **93**, 174 (2001).
17. L. H. Shi, H. Li, Z. X. Wang, X. J. Huang, and L. Q. Chen, *J. Mater. Chem.*, **11**, 1502 (2001).
18. M. J. Fasolka and A. M. Mayes, *Annu. Rev. Mater. Res.*, **31**, 323 (2001); and references therein.
19. Y. C. Chan, G. W. Craig, R. R. Schrock, and R. E. Cohen, *Chem. Mater.*, **4**, 885 (1992).
20. B. H. Sohn and R. E. Cohen, *J. Appl. Polym. Sci.*, **65**, 723 (1997).
21. J. F. Ciebien, R. T. Clay, B. H. Sohn, and R. E. Cohen, *New J. Chem.*, **22**, 685 (1998).
22. Y. Boontongkong, R. E. Cohen, and M. F. Rubner, *Chem. Mater.*, **12**, 1628 (2000).
23. J. P. Spatz, A. Roescher, and M. Möller, *Polym. Prepr. (Am. Chem. Soc. Div. Polym. Chem.)*, **37**, 409 (1996).
24. P. F. W. Simon, R. Ulrich, H. W. Spiess, and U. Wiesner, *Chem. Mater.*, **13**, 3464 (2001).
25. R. Ulrich, A. Du Chesne, M. Templin, and U. Wiesner, *Adv. Mater.*, **11**, 141 (1999).
26. G. D. Brown and J. J. Watkins, *Mater. Res. Soc. Symp. Proc.*, **584**, 169 (2000).
27. C.-G. Wu and T. Bein, *Science*, **264**, 1757 (1994).
28. C. A. Foss, Jr., G. L. Hornyak, J. A. Stockert, and C. R. Martin, *J. Phys. Chem.*, **96**, 7497 (1992).
29. C. J. Patrissi and C. R. Martin, *J. Electrochem. Soc.*, **148**, A1247 (2001).
30. N. Li and C. R. Martin, *J. Electrochem. Soc.*, **148**, A164 (2001).
31. N. Li, C. J. Patrissi, and C. R. Martin, *J. Electrochem. Soc.*, **147**, 2044 (2000).
32. C. R. Martin, *Science*, **266**, 1961 (1994).
33. M. Nishizawa, V. P. Menon, and C. R. Martin, *Science*, **268**, 700 (1995).
34. G. Che, B. B. Lakshmi, E. R. Fisher, and C. R. Martin, *Nature (London)*, **393**, 346 (1998).
35. J. S. Sakamoto and B. Dunn, *J. Electrochem. Soc.*, **149**, A26 (2001).
36. A. S. Claye, J. E. Fischer, C. B. Huffman, A. G. Rinzler, and R. E. Smalley, *J. Electrochem. Soc.*, **147**, 2845 (2000).
37. M. S. Dresselhaus and G. Dresselhaus, *J. Electroceram.*, **1**, 273 (1997).
38. V. A. Nalimova, D. E. Sklovsky, G. N. Bondarenko, H. Alvergnatgaucher, S. Bonnamy, and F. Beguin, *Synth. Met.*, **88**, 89 (1997).
39. E. Frackowiak, S. Gautier, H. Gaucher, S. Bonnamy, and F. Beguin, *Carbon*, **37**, 61 (1999).
40. G. T. Wu, C. W. Wang, X. B. Zhang, H. S. Yang, Z. F. Qi, P. M. He, and W. Z. Li, *J. Electrochem. Soc.*, **146**, 1696 (1999).
41. B. Gao, A. Kleinhammes, X. P. Tang, C. Bower, L. Fleming, Y. Wu, and O. Zhou, *Chem. Phys. Lett.*, **307**, 153 (1999).
42. A. G. Rinzler, J. Liu, H. Dai, P. Nikolaev, C. B. Huffman, F. J. Rodriguez-Macias, P. J. Boul, A. H. Lu, D. Heymann, D. T. Colbert, R. S. Lee, J. E. Fischer, A. Rao, P. Eklund, and R. E. Smalley, *Appl. Phys. A: Mater. Sci. Process.*, **67**, 29 (1998).
43. K. E. Thomas and J. Newman, in *Advanced Batteries and Supercapacitors*, G. Nazri, R. Koetz, B. Scrosati, P. A. Moro, and E. S. Takeuchi, Editors, PV 2001-21, The Electrochemical Society Proceedings Series, Pennington, NJ (2001).
44. K. E. Thomas, Ph.D. Thesis, University of California at Berkeley (Spring 2002).
45. F. M. Gray, J. R. Maccallum, C. A. Vincent, and J. R. M. Giles, *Macromolecules*, **21**, 392 (1988).
46. I. Khan, D. Fish, Y. Delaviz, and J. Smid, *Makromol. Chem.*, **190**, 1069 (1989).
47. P. Soo, B. Huang, Y.-I. Jang, Y.-M. Chiang, D. R. Sadoway, and A. M. Mayes, *J. Electrochem. Soc.*, **146**, 32 (1999).
48. A. V. G. Ruzette, P. P. Soo, D. R. Sadoway, and A. M. Mayes, *J. Electrochem. Soc.*, **148**, A537 (2001).
49. D. R. Sadoway, A. M. Mayes, B. Huang, P. E. Trapa, P. P. Soo, and P. Bannerjee, *J. Power Sources*, **97-98**, 621 (2001).
50. P. C. Trapa, B. Huang, D. R. Sadoway, and A. M. Mayes, *Electrochem. Solid-State Lett.*, **5**, A85 (2002).
51. *Binary Alloy Phase Diagrams*, T. B. Massalski, H. Okamoto, P. R. Subramanian, and L. Kacprzak, Editors, ASM International, Materials Park, OH (1990).
52. J. Huh, V. V. Ginzberg, and A. C. Balazs, *Macromolecules*, **33**, 8085 (2000).
53. R. B. Thompson, V. V. Ginzburg, M. W. Matsen, and A. C. Balazs, *Science*, **292**, 2469 (2001).
54. D. E. Sayers, S. M. Heald, M. A. Pick, J. I. Budnick, E. A. Stern, and J. Wong, *Nucl. Instrum. Methods Phys. Res.*, **208**, 631 (1983).
55. D. E. Sayers and B. A. Bunker, in *X-Ray Absorption: Principles, Applications, Techniques of EXAFS, SEXAFS, and XANES*, D. C. Koningsberger and R. Prins, Editors, Chap. 6, Wiley, New York (1988).
56. J. J. W. Cook and D. E. Sayers, *J. Appl. Phys.*, **52**, 5024 (1981).
57. W. H. McMaster, N. K. D. Grande, J. H. Mallet, and J. H. Hubbell, Lawrence Livermore Final Report UCRL-50174, National Technical Information Services, Springfield, VA (1969).
58. M. I. Lozow, S.B. Thesis, Massachusetts Institute of Technology, Cambridge, MA (1999).
59. K. I. Winey, E. L. Thomas, and L. J. Fetters, *Macromolecules*, **95**, 9367 (1991).
60. H. Hasegawa, H. Tanaka, K. Yamasaki, and T. Hashimoto, *Macromolecules*, **20**, 1651 (1987).
61. A. D. Pelton, *Bull. Alloy Phase Diagrams*, **7**, 228 (1986).
62. B. Predal, in *Numerical Data and Functional Relationships in Science and Technology*, New Series, IV, O. Madelung, Editor, Landolt-Börnstein, New York (1991).
63. H. W. King, *J. Mater. Sci.*, **1**, 79 (1966).
64. M. L. Bhatia, A. K. Singh, and T. K. Nandy, *Intermetallics*, **6**, 141 (1998).
65. G. Kienast and J. Verma, *Z. Anorg. Allg. Chem.*, **320**, 143 (1961).
66. E. Peled, D. Golodnitsky, and J. Penciner, in *Handbook of Battery Materials*, J. O. Besenhard, Editor, Chap 6, Wiley-VCH, Cambridge, U.K. (1999).